

# Vibrational Imaging Techniques and Hard Dental Tissues

Subjects: Biophysics

Contributor: Elisabetta Giorgini, Giovanna Orsini, Giulia Orilisi, Valentina Notarstefano, Riccardo Monterubbianesi, Flavia Vitiello, Vincenzo Tosco, Alessia Belloni, Angelo Putignano

Raman Microspectroscopy (RMS) represents an innovative tool to in vitro situation hard dental tissues. In fact, this vibrational technique has the advantage of providing, at the same time and on the same sample, a morpho-chemical correlation between the microscopic information from the visual analysis of the sample and its chemical and macromolecular composition. Moreover, thanks to the light scattering, it is possible to simultaneously perform the imaging analysis of both the inorganic and organic components of teeth, at a high spatial resolution level and in a confocal mode. The identification of specific Raman markers representative of sound and pathological hard dental tissues is crucial to improve the diagnosis of several dental pathologies and to detect dental lesions at an early stage when they are not visually detectable .

Keywords: Raman Microspectroscopy ; Fourier Transform Infrared spectroscopy ; vibrational spectroscopy ; enamel ; dentin ; hard dental tissues

## 1. RMS and ATR-FTIR Characterization of Hard Dental Tissues

Enamel and dentin are the major components of the human dental crown, whereas dentin and cementum are present in the human dental root. Enamel represents the most mineralized tissue of the human body, with a composition up to 96–97% (by weight) inorganic matter, 2–3% water, and only 1% non-collagenous organic material <sup>[1]</sup>. The main component of the enamel mineral phase is crystalline bundles of hydroxyapatite (HA) in a hexagonal shape; hydroxyapatite is a mineral form of calcium apatite with a chemical formula  $\text{Ca}_5(\text{PO}_4)_3(\text{OH})$ , present in teeth and bones. Enamel mineralization is crucial since a reduction in mineral content could lead to caries susceptibility and dental lesions. Moreover, variation in mineralization may manifest itself through the formation of white spot lesions (WSLs), which also impact teeth aesthetics <sup>[2]</sup>. Dentin is a composite material containing 70% mineral components, in form of mineral nanocrystallites, and 20% protein matrix, predominantly formed by cross-linked type I collagen (90% of the whole dentin protein fraction) <sup>[3]</sup>. Cementum is a mineralized tissue covering the entire root surface and consists of approximately 50% inorganic matrix (HA) and 50% organic matrix (collagen, predominantly type I, and non-collagenous proteins) and water <sup>[4]</sup>.

In-depth knowledge of the extent and severity of dental disorders and alterations of dental structures may provide valuable information for treatment procedures. It has been investigated that the chemical composition of human teeth in terms of decay, demineralization/remineralization processes, and disease using various analytical methods <sup>[5][6][7][8]</sup>. Among all, RMS represents an innovative technique, allowing both inorganic and organic components. Since the spectral profile and the peaks' position can be influenced by composition and structure <sup>[9]</sup>, thus making their interpretation challenging, the detailed analysis of the spectral bands related to the chemical composition of the different dental components is mandatory.

In **Figure 1**, the main IR and Raman bands representative of enamel, dentin, and cementum in sound teeth are reported. Regarding enamel, the main Raman bands are assigned to phosphates ( $\text{PO}_4^{3-}$ ,  $960\text{ cm}^{-1}$ ), and A- ( $\text{CO}_3^{2-}$ ,  $1102\text{ cm}^{-1}$ ) and B-type ( $\text{CO}_3^{2-}$ ,  $1070\text{ cm}^{-1}$ ) carbonate groups in HA <sup>[10]</sup>, with the latter representing the  $\nu_1$  symmetric stretching mode of  $\text{CO}_3^{2-}$  ions replacing  $\text{PO}_4^{3-}$  in the apatite lattice <sup>[11]</sup>. Carbonate substitution affects HA in terms of solubility and reactivity <sup>[12]</sup>. Significant changes in the intensities of these bands were found in carious lesions with respect to healthy enamel and were mainly attributed to demineralization-induced alterations of enamel crystallite morphology and/or orientation <sup>[13][14]</sup>. It is well known that crystallinity increases when crystals are larger and/or more perfect, and when there is less substitution <sup>[15]</sup>. Moreover, in Raman enamel spectra, a weak band at  $1660\text{ cm}^{-1}$ , attributable to the amide I band and hence to the organic matrix, can be detected. The Raman spectrum of dentin is characterized by bands at  $1660\text{ cm}^{-1}$ ,  $1450\text{ cm}^{-1}$ , and  $1242\text{ cm}^{-1}$  (attributable to collagen) and  $1070\text{ cm}^{-1}$  ( $\text{CO}_3^{2-}$ ) and  $960\text{ cm}^{-1}$  ( $\text{PO}_4^{3-}$  of hydroxyapatite).

Finally, cementum shows Raman bands at  $960\text{ cm}^{-1}$ , and  $1452\text{ cm}^{-1}$  and  $1660\text{ cm}^{-1}$ , the first assigned to the mineral component and the other two to the organic matrix [13].

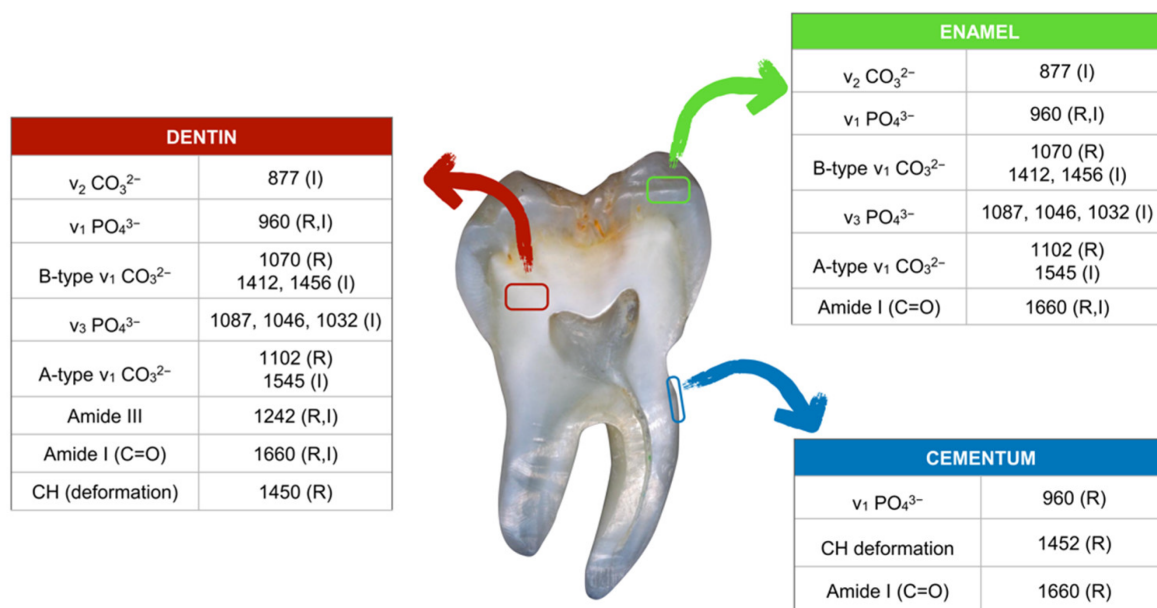


**Figure 1.** Main Raman (R) and IR (I) peaks of enamel, dentin, and cementum, together with the corresponding vibrational modes (v: stretching vibration).

By the analysis of Raman spectra, some parameters, such as the full width at half maximum of a single band (FWHM) and band ratios obtained using the areas (A) or the intensities (I) of the most significant bands, can be calculated and used as markers to provide accurate diagnostic information related to diseases affecting dental tissues (**Figure 2**). Among all, the main analyzed parameters are mineral/matrix ( $A_{960}/A_{1660}$ ), crystallinity (inversely proportional to  $\text{FWHM}_{960}$ ), P ( $I_{960}$ ), and carbonate-to-phosphate ratio (C/P) or gradient in mineral content (GMC) ( $I_{1070}/I_{960}$ ) [16]. The mineral/matrix ratio (M/M) is related to the amount of the mineral component with respect to the organic one. It is calculated as the ratio between the area of the band at  $960\text{ cm}^{-1}$ , which is the most intense mineral band of HA (attributed to phosphates), and that of the amide I band centered at  $1660\text{ cm}^{-1}$  [17]. This ratio is used to describe the mineral transitions in affected carious dentine, from the transparent zone into the normal zone [18]. Indeed, Liu et al. found that the mineral component is higher within the sub-transparent zone than in normal and transparent zones [18]. Crystallinity (C) is correlated with the degree of order within the mineral crystals and represents a critical component of HA, since ion substitution may introduce structural distortions. This parameter is directly proportional to the inverse of the full width at half maximum (FWHM) of the above-mentioned band centered at  $960\text{ cm}^{-1}$ , meaning that a narrow band width indicates a high mineral crystallinity and vice versa [3]. In the studies reported by Al-Obaidi et al. and Slimani et al., the degree of C was determined in enamel by measuring changes in the peaks ratio of the symmetric mode of phosphate at  $960\text{ cm}^{-1}$  over  $950\text{ cm}^{-1}$  [19][20]. The carbonate-to-phosphate ratio (C/P), or gradient in mineral content (GMC), calculated as the ratio between the intensities of the bands centered at  $1070\text{ cm}^{-1}$  and  $960\text{ cm}^{-1}$  attributed to carbonate and phosphate groups in HA, respectively, indicates the extent of carbonate incorporation in the HA lattice, and curve-fitting of the carbonate band reveals whether the carbonate has replaced hydroxide (A-type) or phosphate (B-type) in the apatite lattice. During the demineralization process, a progressive increase of C/P occurs, due to the substitution of  $\text{CO}_3^{2-}$  for  $\text{PO}_4^{3-}$  in HA (type B substitution) [20][21]. Almhöjd et al. observed different values of this ratio in sound and carious dentine, the latter showing lower values with respect to sound dentine. In addition, the intensity of the peaks at  $1246\text{ cm}^{-1}$ ,  $1450\text{ cm}^{-1}$ , and  $1655\text{ cm}^{-1}$  (attributed to amide III,  $\text{CH}_2$  groups, and amide I, respectively) are employed to evaluate structural organization and relative amount of collagen. In more detail, the amide I/amide III ratio (calculated as the ratio between the area of amide I and amide III bands) is related to collagen organization, while the amide III/ $\text{CH}_2$  and amide I/ $\text{CH}_2$  ratios indicate differences in collagen structure and quality [22][23].

MINERAL / MATRIX	$(A_{960}/A_{1660})$	Amount of the mineral component respect to the organic one
CRYSTALLINITY	$(1/\text{FWHM}_{960})$	Degree of order within the HA mineral crystals
CARBONATE/ PHOSPHATE	$(I_{1070}/I_{960})$	Extent of carbonate incorporation in the hydroxyapatite lattice
PHOSPHATES	$(I_{960})$	Mineral compound of HA
CH <sub>2</sub> GROUPS	$(I_{1450})$	Structural organization and relative amount of collagen
AMIDE I	$(I_{1655})$	
AMIDE III	$(I_{1246})$	
AMIDE I / AMIDE III	$(I_{1655}/I_{1246})$	Collagen organization
AMIDE III / CH <sub>2</sub>	$(I_{1246}/I_{1450})$	Differences in collagen structure and quality
AMIDE I / CH <sub>2</sub>	$(I_{1655}/I_{1450})$	

**Figure 2.** Raman-derived markers for the characterization of hard dental tissues (I: intensity of the band; A: area of the band; and FWHM: full width at half maximum).

## 2. RMS Characterization of Dental Lesions

Hard dental tissues can be subjected to different factors that influence the normal chemical phenotype. Amelogenesis (AI) and dentinogenesis (DI) imperfectae represent a heterogeneous group of genetic conditions characterized by defects in the formation of enamel and dentin, respectively, in teeth of both dentitions [24][25]. On the other hand, enamel and dentin mineralization can be affected, after their eruption, by different extrinsic factors, such as poor oral hygiene, alcohol and acidic beverage consumption, high intake of dietary carbohydrates, and dental trauma, all leading to early demineralization [26]. Moreover, if these lesions are not stopped or reversed through non-invasive treatments, they can evolve from early enamel lesions to dental caries, affecting both the enamel and dentin.

The relation between the main spectral features and the most frequent diseases of hard dental tissues is shown in **Figure 3** and described in the paragraphs below.

MINERAL / MATRIX	$(A_{960}/A_{1660})$	Amount of the mineral component respect to the organic one
CRYSTALLINITY	$(1/FWHM_{960})$	Degree of order within the HA mineral crystals
CARBONATE/ PHOSPHATE	$(I_{1070}/I_{960})$	Extent of carbonate incorporation in the hydroxyapatite lattice
PHOSPHATES	$(I_{960})$	Mineral compound of HA
CH <sub>2</sub> GROUPS	$(I_{1450})$	Structural organization and relative amount of collagen
AMIDE I	$(I_{1655})$	
AMIDE III	$(I_{1246})$	
AMIDE I / AMIDE III	$(I_{1655}/I_{1246})$	Collagen organization
AMIDE III / CH <sub>2</sub> AMIDE I / CH <sub>2</sub>	$(I_{1246}/I_{1450})$ $(I_{1655}/I_{1450})$	Differences in collagen structure and quality

**Figure 3.** Variations of the main Raman-derived spectral parameters in relation to different dental pathologies (WSLs: white spot lesions; D: dentin; DC: dental caries; AI: amelogenesis imperfecta; DI: dentinogenesis imperfecta).

## 2.1. RMS of Amelogenesis and Dentinogenesis Imperfectae

The evaluation of enamel and dentin mineralization could be useful of dental genetic anomalies, such as AI and DI [27]. Wright et al. reported increased levels of protein in AI enamel, even up to 30% in some types, with respect to sound enamel; however, no significant differences were found in the carbonate content between AI and sound enamel. Moreover, Bērziņš et al., it was suggested that a severely degraded AI tooth appeared to still include a small tier of highly ordered HA [28]. In another, C/P was found to be significantly higher in AI teeth compared to sound teeth [29].

For DI, dentin possesses higher peak intensities of phosphate and amide III bands than normal dentin [30]. However, no significant differences were observed in the peak intensities of carbonate between DI and normal dentin. Additionally, C/P or GMC (carbonate-to-phosphate ratio or gradient in mineral content) was used to measure differences in relative composition, and a significant increment of GMC was found in DI-II dentin compared to normal dentin. Moreover, the ratio of amide I to amide III, relating to the organization of collagen, resulted in increased DGI-II dentin compared to normal dentin [30].

## 2.2. RMS Characterization of Early Enamel Lesions

RMS is a valuable tool to detect carious lesions at an early stage of formation, since it allows for the collection of high-resolution maps and is highly sensitive to small changes in enamel composition [10].

The first clinically visible stage of carious disease is characterized by enamel demineralization without cavitation, known as white spot lesions (WSLs). However, in the absence of effective treatment, cavitation may occur, thereby increasing the necessity of invasive restorative treatments [31]. WSLs appear as milky white opaque spots on dental enamel. The translucency of enamel is an optical phenomenon that depends on the size of the intercrystalline spaces. In early stages, active caries require air drying to be visible, as the dissolution process of crystals at the outer enamel surface begins. Further enlargement of intercrystalline spaces results in a white patch that is visible without dryness. The effect of dehydration on enamel translucency is a result of the replacement of water content around enamel prisms with air. In a heterogeneous system, such as enamel prisms surrounded by a fluid medium, scattering occurs due to differences in the refractive indices (RI) of the two involved components. As the RI of enamel is approximately 1.65, while that of water is 1.33 and that of air is 1.00, a greater difference among RI values produces a greater scattering at the enamel/air interface.

Ko et al. and Kinoshita et al. successfully provided Raman spectral imaging characterization for early caries [32][33]. Indeed, the high spatial resolution (300 nm) makes it an excellent tool for analyzing human enamel components, enabling the detection of WSLs at an early stage of development [34]. In order to define the levels of enamel demineralization after exposure to acid environments, it has been analyzed that the width of the bands related to phosphate vibrations (such as the band centered at  $960\text{ cm}^{-1}$ ) [35].

Recently, chemical mapping of dental enamel was carried out over cross sections of specimens with natural and artificial WSLs [40]. It was observed a severe decrease in the intensity of the  $\text{PO}_4^{3-}$  peak in the area corresponding to the body of the lesion, with respect to sound enamel. A similar trend was shown by C, which abruptly decreases in the lesion zone, while it starts to gradually increase in the intermediate zone, reaching its maximum value in sound enamel beyond the subsurface lesion. These findings are related to some alteration in crystal size and shape and, consequently, to reduced apatite perfection of the enamel prism. Finally, false color images derived from the  $\text{CO}_3^{2-}/\text{PO}_4^{3-}$  ratio, used to analyze changes in enamel inorganic components in each zone of the lesion, revealed an increase in the ratio in the lesion, in comparison to sound enamel. Hence, it can be stated that in WSLs, enamel becomes less compact due to the increase of inter-prismatic voids, and less mineralized due to the decrease in mineral density and the increase in the organic matrix content [10].

### 2.3. RMS Characterization of Dental Caries

Dental caries is one of the most prevalent chronic diseases worldwide, affecting people throughout their lifetime. It is an irreversible microbial disease that affects the calcified structures of the tooth. Despite several preventive measures aiming to reduce the incidence of this pathology, such as careful dental hygiene and the addition of fluorine to drinking water, the occurrence of caries is still one of the most common diseases experienced by most individuals. It is known that the organic component can act as an inhibitor of hydroxyapatite crystals' growth during the processes of formation and development of caries, causing organic and inorganic biochemical alterations [18][36]. Therefore, a detailed analysis of these biochemical changes is mandatory to assess the best approach to help with remineralization of compromised dental tissue [37].

There is a need to develop new methods able to identify the presence of enamel caries before it is detectable with routine assays. RMS may provide this by characterizing the biochemical composition of healthy and carious enamel and dentine [38]. An in vitro one reported that polarized RMS showed a sensitivity of 97% and a specificity of 100% for the detection of caries [32]. Moreover, another recent one was concluded that RMS can be used as a non-contact analytical technology for in vitro studies to discriminate with high resolution the zones of carious dentin tissues by using the amide I/phosphate  $\nu_1$  band ratio, calculated as the ratio between the areas of the bands at  $1655\text{ cm}^{-1}$  and  $960\text{ cm}^{-1}$ , related to amide I of proteins and  $\nu_1$  of phosphates, respectively [39].

Previously, the polarized Raman spectra of enamel, obtained after excitation with the 785 nm laser beam, was used to calculate the depolarization ratio and polarization anisotropy for distinguishing early carious processes. In sound enamel, apatite crystals are ordered in one direction, perpendicular to the enamel surface; in the presence of caries, this ordered arrangement is altered and the structure appears more disordered with enamel crystals that are not parallel to each other. In sound enamel, the depolarization ratio is low and the polarization anisotropy is high; conversely, the first increases and the latter decreases due to disordered carious enamel structure [40]. Buchwald et al., it was highlighted some differences in the intensity, position, and FWHM of the  $\nu_1$  band of phosphates at  $960\text{ cm}^{-1}$  between sound and carious enamel. The simultaneous decreases of the value of the band intensity and FWHM were associated with a lower amount of apatite crystals in carious enamel [40]. It is important to check how these band parameters are affected by early demineralization of sound enamel under controlled conditions in order to define RMS as a reliable diagnostic tool in dentistry. Buchwald et al. observed that the values of the band position increase with enamel demineralization, and this shift to higher wavenumbers was attributed to changes in the vibrational energy of apatite crystals in demineralized enamel. These spectral modifications were also associated with a decrease in the amount of enamel phosphate and a reduction of the order of the structure [40].

Das Gupta et al. reported RMS chemical maps of enamel and dentin caries infiltration [41]. The enamel lesions appeared to be less mineralized due to more substituted carbonate in the crystal lattice compared to the sound enamel. When the lesion extends into the dentin, tissues have less mineral content than the sound dentin; however, many mineral apatites of caries are more crystalline and hence have less substituted carbonate in the lattice. Moreover, carious lesions have higher C than the dentin but lower C than enamel, and higher carbonate substitution in the lattice than enamel and dentin, which indicates the presence of crystals with less stoichiometric perfection in the caries lesion. In carious enamel, together with a decrease in the intensity of Raman peaks, differences in terms of band positions were also observed [40].

During the demineralization process in dentin, the band at  $960\text{ cm}^{-1}$  becomes progressively lower, while the bands related to the organic component (amide I and amide III bands) did not show any change due to the acidic environment, thus proving that there is a progressive decrease in the fraction of the mineral phase with respect to that of the collagenous matrix [42]. Interestingly, the remineralization process appeared to increase the relative intensity of the  $\text{PO}_4^{3-}$  bands only when dentin samples were treated in acidic solutions for less than 12 h. As the pH of the demineralizing environment was decreased to a value of 2, the Raman intensity of the phosphate bands was further reduced, and samples lost the ability to recover any mineralization after just 6 h of acidic treatment. During demineralization, a non-linear correlation was found between the M/M band ratio and C: M/M decreases with the square power of  $\text{FWHM}_{960}$  [42]. The decrease in M/M at a rate faster than the linear rate let hypothesize that the main rate-controlling phenomenon for structural recovery during remineralization is the deposition of new mineral crystals [42].

---

## References

1. Rodrigo S. Lacruz; Stefan Habelitz; J. Timothy Wright; Michael L. Paine; Dental Enamel Formation and Implications for Oral Health and Disease. *Physiological Reviews* **2017**, 97, 939-993, [10.1152/physrev.00030.2016](https://doi.org/10.1152/physrev.00030.2016).
2. Kamna Srivastava; Tripti Tikku; Rohit Khanna; Kiran Sachan; Risk factors and management of white spot lesions in orthodontics. *Journal of orthodontic science* **2013**, 2, 43-49, [10.4103/2278-0203.115081](https://doi.org/10.4103/2278-0203.115081).
3. M. Anwar Alebrahim; C. Krafft; W. Sekhaneh; B. Sigusch; J. Popp; ATR-FTIR and Raman spectroscopy of primary and permanent teeth. *Biomedical Spectroscopy and Imaging* **2014**, 3, 15-27, [10.3233/BSI-130059](https://doi.org/10.3233/BSI-130059).
4. Tsuneyuki Yamamoto; Tomoka Hasegawa; Tomomaya Yamamoto; Hiromi Hongo; Norio Amizuka; Histology of human cementum: Its structure, function, and development. *Japanese Dental Science Review* **2016**, 52, 63-74, [10.1016/j.jdsr.2016.04.002](https://doi.org/10.1016/j.jdsr.2016.04.002).
5. R.P. Shellis; Relationship between human enamel structure and the formation of caries-like lesions in vitro. *Archives of Oral Biology* **1984**, 29, 975-981, [10.1016/0003-9969\(84\)90144-4](https://doi.org/10.1016/0003-9969(84)90144-4).
6. Agr Targino; Aronita Rosenblatt; Andressa Oliveira; Amb Chaves; Ve Santos; The relationship of enamel defects and caries: a cohort study. *Oral Diseases* **2010**, 17, 420-426, [10.1111/j.1601-0825.2010.01770.x](https://doi.org/10.1111/j.1601-0825.2010.01770.x).
7. Neslihan Efeoglu; David Wood; Candan Efeoglu; Microcomputerised tomography evaluation of 10% carbamide peroxide applied to enamel. *Journal of Dentistry* **2005**, 33, 561-567, [10.1016/j.jdent.2004.12.001](https://doi.org/10.1016/j.jdent.2004.12.001).
8. Neslihan Efeoglu; David J. Wood; Candan Efeoglu; Thirty-five percent carbamide peroxide application causes in vitro demineralization of enamel. *Dental Materials* **2007**, 23, 900-904, [10.1016/j.dental.2006.06.032](https://doi.org/10.1016/j.dental.2006.06.032).
9. G. Penel; G. Leroy; C. Rey; E. Bres; MicroRaman Spectral Study of the PO 4 and CO 3 Vibrational Modes in Synthetic and Biological Apatites. *Calcified Tissue Research* **1998**, 63, 475-481, [10.1007/s002239900561](https://doi.org/10.1007/s002239900561).
10. R. Al-Obaidi; H. Salehi; A. Desoutter; L. Bonnet; P. Etienne; E. Terror; B. Jacquot; B. Levallois; H. Tassery; F. J. G. Cuisinier; et al. Chemical & Nano-mechanical Study of Artificial Human Enamel Subsurface Lesions. *Scientific Reports* **2018**, 8, 1-8, [10.1038/s41598-018-22459-7](https://doi.org/10.1038/s41598-018-22459-7).
11. Ozlem Marti Akgun; Sevgi Haman Bayari; Semra Ide; Gunseli Guven Polat; Ceren Yildirim; Ilgar Orujalipoor; Evaluation of the protective effect on enamel demineralization of CPP-ACP paste and ROCS by vibrational spectroscopy and SAXS : An in vitro study. *Microscopy Research and Technique* **2021**, 84, 2977–2987, [10.1002/jemt.23857](https://doi.org/10.1002/jemt.23857).
12. Mark T. Fulmer; Ira C. Ison; Christine R. Hankermayer; Brent R. Constantz; John Ross; Measurements of the solubilities and dissolution rates of several hydroxyapatites. *Biomaterials* **2002**, 23, 751-755, [10.1016/s0142-9612\(01\)0180-6](https://doi.org/10.1016/s0142-9612(01)0180-6).
13. Ravikumar Ramakrishnaiah; Ghufuran Ur Rehman; Santhosh Basavarajappa; Abdulaziz Abdullah Al Khuraif; B. H. Durgesh; Abdul Samad Khan; Ihtesham Ur Rehman; Applications of Raman Spectroscopy in Dentistry: Analysis of Tooth Structure. *Applied Spectroscopy Reviews* **2014**, 50, 332-350, [10.1080/05704928.2014.986734](https://doi.org/10.1080/05704928.2014.986734).
14. Ana Flávia Sanches Borges; Renata Andrade Bitar; Kamila Rosamilia Kantovitz; Américo Bortollazo Correr; Airtton Abrahão Martin; Regina Maria Puppim-Rontani; New perspectives about molecular arrangement of primary and permanent dentin. *Applied Surface Science* **2007**, 254, 1498-1505, [10.1016/j.apsusc.2007.07.018](https://doi.org/10.1016/j.apsusc.2007.07.018).
15. Changqi Xu; Rosi Jan Reed; Jeffrey P. Gorski; Yiguo Wang; Mary P. Walker; The distribution of carbonate in enamel and its correlation with structure and mechanical properties. *Journal of Materials Science* **2012**, 47, 8035-8043, [10.1007/s10853-012-6693-7](https://doi.org/10.1007/s10853-012-6693-7).
16. Giulia Orilisi; Riccardo Monterubbianesi; Valentina Notarstefano; Vincenzo Tosco; Flavia Vitiello; Giampaolo Giuliani; Angelo Putignano; Giovanna Orsini; New insights from Raman MicroSpectroscopy and Scanning Electron Microscopy

on the microstructure and chemical composition of vestibular and lingual surfaces in permanent and deciduous human teeth. *Spectrochimica Acta Part A: Molecular and Biomolecular Spectroscopy* **2021**, *260*, 119966, [10.1016/j.saa.2021.119966](https://doi.org/10.1016/j.saa.2021.119966).

17. Mohamed Khalid; Tanujjal Bora; Ahmed Al Ghaithi; Sharanjit Thukral; Joydeep Dutta; Raman Spectroscopy detects changes in Bone Mineral Quality and Collagen Cross-linkage in Staphylococcus Infected Human Bone. *Scientific Reports* **2018**, *8*, 1-9, [10.1038/s41598-018-27752-z](https://doi.org/10.1038/s41598-018-27752-z).
18. Y.W. Liu; Xin Yao; Yunxia Wang; A Fourier Transform Infrared Spectroscopy Analysis of Carious Dentin from Transparent Zone to Normal Zone. *Caries Research* **2014**, *48*, 320-329, [10.1159/000356868](https://doi.org/10.1159/000356868).
19. Amel Slimani; Fares Nouioua; Alban Desoutter; Bernard Levallois; Frédéric J. G. Cuisinier; Hervé Tassery; Elodie Terror; Hamideh Salehi; Confocal Raman mapping of collagen cross-link and crystallinity of human dentin–enamel junction. *Journal of Biomedical Optics* **2017**, *22*, 086003, [10.1117/1.jbo.22.8.086003](https://doi.org/10.1117/1.jbo.22.8.086003).
20. Tattiana Enrich-Essvein; Cristina Benavides-Reyes; Pedro Álvarez-Lloret; María Victoria Bolaños-Carmona; Alejandro B. Rodríguez-Navarro; Santiago González-López; Influence of de-remineralization process on chemical, microstructural, and mechanical properties of human and bovine dentin. *Clinical Oral Investigations* **2020**, *25*, 841-849, [10.1007/s00784-020-03371-9](https://doi.org/10.1007/s00784-020-03371-9).
21. Antonio José Ortiz-Ruiz; Juan De Dios Teruel-Fernández; Luis Alberto Alcolea-Rubio; Ana Hernández-Fernández; Yolanda Martínez-Beneyto; Francesc Gispert Guirado; Structural differences in enamel and dentin in human, bovine, porcine, and ovine teeth. *Annals of Anatomy - Anatomischer Anzeiger* **2018**, *218*, 7-17, [10.1016/j.aanat.2017.12.012](https://doi.org/10.1016/j.aanat.2017.12.012).
22. Hamideh Salehi; Elodie Terror; Ivan Panayotov; Bernard Levallois; Bruno Jacquot; Hervé Tassery; Frédéric Cuisinier; Functional mapping of human sound and carious enamel and dentin with Raman spectroscopy. *Journal of Biophotonics* **2012**, *6*, 765-774, [10.1002/jbio.201200095](https://doi.org/10.1002/jbio.201200095).
23. Manuel Toledano; Fátima S. Aguilera; Estrella Osorio; Inmaculada Cabello; Manuel Toledano-Osorio; Raquel Osorio; Functional and molecular structural analysis of dentine interfaces promoted by a Zn-doped self-etching adhesive and an in vitro load cycling model. *Journal of the Mechanical Behavior of Biomedical Materials* **2015**, *50*, 131-149, [10.1016/j.jmbbm.2015.05.026](https://doi.org/10.1016/j.jmbbm.2015.05.026).
24. Claire E. L. Smith; James Poulter; Agne Antanaviciute; Jennifer Kirkham; Steven Brookes; Chris F. Inglehearn; Alan J. Mighell; Amelogenesis Imperfecta; Genes, Proteins, and Pathways. *Frontiers in Physiology* **2017**, *8*, 435-435, [10.3389/fphys.2017.00435](https://doi.org/10.3389/fphys.2017.00435).
25. K. Gadhia; S. McDonald; N. Arkutu; K. Malik; Amelogenesis imperfecta: an introduction. *British Dental Journal* **2012**, *212*, 377-379, [10.1038/sj.bdj.2012.314](https://doi.org/10.1038/sj.bdj.2012.314).
26. Anna Akkus; Asya Akkus; Renato Roperto; Ozan Akkus; Thiago Porto; Sorin Teich; Lisa Lang; Evaluation of mineral content in healthy permanent human enamel by Raman spectroscopy. *Journal of Clinical and Experimental Dentistry* **2016**, *8*, e546-e549, [10.4317/jced.53057](https://doi.org/10.4317/jced.53057).
27. G. Orsini; A. Majorana; A. Mazzoni; A. Putignano; M. Falconi; A. Polimeni; L. Breschi; Immunocytochemical detection of dentin matrix proteins in primary teeth from patients with dentinogenesis imperfecta associated with osteogenesis imperfecta. *European Journal of Histochemistry* **2014**, *58*, 2405, [10.4081/ejh.2014.2405](https://doi.org/10.4081/ejh.2014.2405).
28. Kārlis Bērziņš; Joshua J. Sutton; Carolina Loch; Deanna Beckett; Benjamin J. Wheeler; Bernadette K. Drummond; Sara J. Fraser-Miller; Keith C. Gordon; Application of low-wavenumber Raman spectroscopy to the analysis of human teeth. *Journal of Raman Spectroscopy* **2019**, *50*, 1375-1387, [10.1002/jrs.5648](https://doi.org/10.1002/jrs.5648).
29. Felicity A. Crombie; David Manton; Joseph E.A. Palamara; Ilya Zaluzniak; Nathan J. Cochrane; Eric C. Reynolds; Characterisation of developmentally hypomineralised human enamel. *Journal of Dentistry* **2013**, *41*, 611-618, [10.1016/j.jdent.2013.05.002](https://doi.org/10.1016/j.jdent.2013.05.002).
30. Jiajie Mao; Lin Wang; Yun Jiang; Haoran Cheng; Ning Li; Shi Shi; Fan Fan; Jianfeng Ma; Shengbin Huang; Nanoscopic wear behavior of dentinogenesis imperfecta type II tooth dentin. *Journal of the Mechanical Behavior of Biomedical Materials* **2021**, *120*, 104585, [10.1016/j.jmbbm.2021.104585](https://doi.org/10.1016/j.jmbbm.2021.104585).
31. Fredrik Bergstrand; Svante Twetman; A Review on Prevention and Treatment of Post-Orthodontic White Spot Lesions - Evidence-Based Methods and Emerging Technologies. *The Open Dentistry Journal* **2011**, *5*, 158-162, [10.2174/1874210601105010158](https://doi.org/10.2174/1874210601105010158).
32. Alex C.-T. Ko; Lin-P'ing Choo-Smith; Mark Hewko; Michael Sowa; Cecilia C. S. Dong; Blaine Cleghorn; Detection of early dental caries using polarized Raman spectroscopy. *Optics Express* **2006**, *14*, 203-215, [10.1364/opex.14.000203](https://doi.org/10.1364/opex.14.000203).
33. H. Kinoshita; N. Miyoshi; Y. Fukunaga; T. Ogawa; T. Ogasawara; K. Sano; Functional mapping of carious enamel in human teeth with Raman microspectroscopy. *Journal of Raman Spectroscopy* **2008**, *39*, 655-660, [10.1002/jrs.1908](https://doi.org/10.1002/jrs.1908).

34. Alban Desoutter; Amel Slimani; Rand Al-Obaidi; Stephane Barthélemy; Frederic Cuisinier; Hervé Tassery; Hamideh Salehi; Cross striation in human permanent and deciduous enamel measured with confocal Raman microscopy. *Journal of Raman Spectroscopy* **2019**, *50*, 548-556, [10.1002/jrs.5555](https://doi.org/10.1002/jrs.5555).
35. Giuseppe Pezzotti; Tetsuya Adachi; Isabella Gasparutti; Giulio Vincini; Wenliang Zhu; Marco Boffelli; Alfredo Rondinella; Elia Marin; Hiroaki Ichioka; Toshiro Yamamoto; et al. Vibrational monitor of early demineralization in tooth enamel after in vitro exposure to phosphoric liquid. *Spectrochimica Acta Part A: Molecular and Biomolecular Spectroscopy* **2017**, *173*, 19-33, [10.1016/j.saa.2016.08.036](https://doi.org/10.1016/j.saa.2016.08.036).
36. Pavel Seredin; Dmitry Goloshchapov; Tatiana Prutskij; Yury Ippolitov; Phase Transformations in a Human Tooth Tissue at the Initial Stage of Caries. *PLoS ONE* **2015**, *10*, e0124008-e0124008, [10.1371/journal.pone.0124008](https://doi.org/10.1371/journal.pone.0124008).
37. Giovanna Orsini; Vincenzo Tosco; Riccardo Monterubbianesi; Scilla Sparabombe; Giulia Orilisi; Angelo Putignano; In Vitro Investigation of the Effect of Different Remineralizing Agents on Human Enamel. *Modern Approaches in Dentistry and Oral Health Care* **2020**, *4*, 369-375, [10.32474/madohc.2020.04.000189](https://doi.org/10.32474/madohc.2020.04.000189).
38. Masatoshi Ando; Chien-Sheng Liao; George J. Eckert; Ji-Xin Cheng; Imaging of demineralized enamel in intact tooth by epideTECTED stimulated Raman scattering microscopy. *Journal of Biomedical Optics* **2018**, *23*, 105005, [10.1117/1.jbo.23.10.105005](https://doi.org/10.1117/1.jbo.23.10.105005).
39. M. Alturki; G. Koller; F. Warburton; U. Almhöjd; A. Banerjee; Biochemical characterisation of carious dentine zones using Raman spectroscopy. *Journal of Dentistry* **2020**, *105*, 103558, [10.1016/j.jdent.2020.103558](https://doi.org/10.1016/j.jdent.2020.103558).
40. Tomasz Buchwald; Zuzanna Buchwald; Assessment of the Raman spectroscopy effectiveness in determining the early changes in human enamel caused by artificial caries. *The Analyst* **2018**, *144*, 1409-1419, [10.1039/c8an01494a](https://doi.org/10.1039/c8an01494a).
41. Shuvashis Das Gupta; Markus Killenberger; Tarja Tanner; Lassi Rieppo; Simo Saarakkala; Jarkko Heikkilä; Vuokko Anttonen; Mikko A. J. Finnilä; Mineralization of dental tissues and caries lesions detailed with Raman microspectroscopic imaging. *The Analyst* **2020**, *146*, 1705-1713, [10.1039/d0an01938k](https://doi.org/10.1039/d0an01938k).
42. Elia Marin; Noriko Hiraishi; Taigi Honma; Francesco Boschetto; Matteo Zanocco; Wenliang Zhu; Tetsuya Adachi; Narisato Kanamura; Toshiro Yamamoto; Giuseppe Pezzotti; et al. Raman spectroscopy for early detection and monitoring of dentin demineralization. *Dental Materials* **2020**, *36*, 1635-1644, [10.1016/j.dental.2020.10.005](https://doi.org/10.1016/j.dental.2020.10.005).

---

Retrieved from <https://encyclopedia.pub/entry/history/show/53613>